Lattice Boltzmann equation with multiple effective relaxation times for gaseous microscale flow

Zhaoli Guo,* Chuguang Zheng, and Baochang Shi
National Laboratory of Coal Combustion, Huazhong University of Science and Technology, Wuhan 430074, People's Republic of China
(Received 29 October 2007; published 21 March 2008)

The standard lattice Boltzmann equation (LBE) is inadequate for simulating gas flows with a large Knudsen number. In this paper we propose a generalized lattice Boltzmann equation with effective relaxation times based on a recently developed generalized Navier-Stokes constitution [Guo *et al.*, Europhys Lett. **80**, 24001 (2007)] for nonequilibrium flows. A kinetic boundary condition corresponding to a generalized second-order slip scheme is also designed for the model. The LBE model and the boundary condition are analyzed for a unidirectional flow, and it is found that in order to obtain the generalized Navier-Stokes equations, the relaxation times must be properly chosen and are related to the boundary condition. Numerical results show that the proposed method is able to capture the Knudsen layer phenomenon and can yield improved predictions in comparison with the standard lattice Boltzmann equation.

DOI: 10.1103/PhysRevE.77.036707 PACS number(s): 47.11.−j, 47.45.−n, 47.61.Cb

I. INTRODUCTION

Small-scale gaseous flows under atmospheric pressure have received particular attention in recent years with the rapid development in microscience and nanoscience and technology [1–3]. The mean free path of the gas, say λ, is usually not very small in comparison with the characteristic length of the flow regions, L. As such, the Knudsen number of the flow, $\mathrm{Kn}=\lambda/L$, may be relatively large, and the continuum assumption may break down. Consequently, the Navier-Stokes equations based on the continuum assumption will fail to work for such flows.

On the other hand, it is well accepted that the Boltzmann equation can be used to model gas flows ranging from the continuum regime ($\mathrm{Kn}<0.001$) to free molecular regime ($\mathrm{Kn}>10$) [4]. Therefore, the Boltzmann equation can serve as a good base for developing reasonable numerical methods for microscale gas flows. Actually, some methods based on the Boltzmann equation have been proposed recently [5–8]. Particularly, the lattice Boltzmann equation (LBE) method has been receiving increasing interests since 2002 [7–22]. However, the applications of the LBE for microscale gas flows are still very premature, and some recent studies have revealed that most of the available LBE models for microflows are inadequate for flows in the transition regime ($\mathrm{Kn}>0.1$) [21,22].

The failure of the standard LBE for high-Kn flows can be attributed to its insufficient capability for capturing the Knudsen layer (KL) or the kinetic boundary layer near solid surfaces. The thickness of the KL is usually in the order of the mean free path of the gas. Outside the KL the collisions between gas molecules are sufficient and the Navier-Stokes equations can be used to describe the gas motion. Within the KL, however, the intermolecular collisions become insufficient so that the quasithermodynamic-equilibrium assumption, upon which the Navier-Stokes equations depend, does not hold any more, and the Navier-Stokes model will fail to work. Since the standard LBE is only accurate at the Navier-Stokes level as an approximation to the Boltzmann equation [21–24], or in other words a numerical scheme for the Navier-Stokes equations, it is not surprising that the standard LBE is incapable of describing the KL, and will fail to work for high-Kn flows where the KL takes a large portion of flow domain.

Recently some efforts have been made to improve the capability of LBE for high-Kn flows. One approach, and perhaps the most natural way, is to increase the approximation accuracy to the continuous Boltzmann equation (CBE), since the LBE is a discrete approximation to the CBE that is capable of describing a gas flow both in and outside the KL. The most challenging aspect of this approach lies in the need to obtain a discrete-velocity set with sufficient symmetry so that discrete moments can match the continuous counterparts at a higher order than the Navier-Stokes levels. Some ways for obtaining a high-order discrete-velocity set have been proposed recently [19,22]. It has been shown that the high-order LBE models can improve the predictions for nonequilibrium flows [22,25,26], but two problems may hinder the applications of this method: First, usually we have no *a priori* knowledge on what the order of the discrete velocity set should be for a specific flow, and second, the use of a high-order discrete-velocity set usually means a large computational cost.

Another approach for capturing the KL with the LBE framework is to make use of an effective relaxation time. As shown in Ref. [21], the collisions between the gas molecules and the solid wall have a significant influence on the mean free path for a confined gas, and thus the relaxation time(s). Therefore, by using an effective relaxation time in which the effects of the gas-solid interaction are taken into account, it is possible to capture the KL within the usual LBE framework. Some recent independent studies have shown that the Navier-Stokes-aimed LBE models with an effective relaxation time can indeed improve the flow predictions within the KL [20,21]. The most critical issue of the effective-relaxation-time method is how to obtain a reasonable effective relaxation time.

The objective of the present work is to develop a generalized LBE model with multiple effective relaxation times for gaseous microscale flows within the standard LBE frame-

*Corresponding author: zlguo@mail.hust.edu.cn

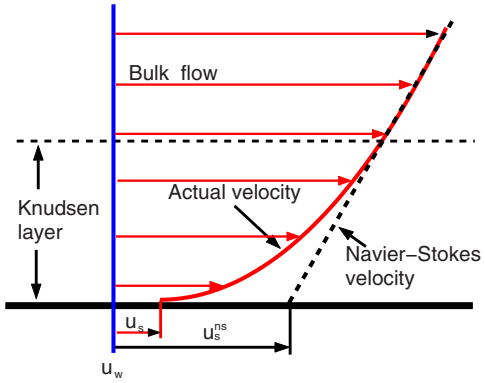

FIG. 1. (Color online) Schematic of the Knudsen layer.

work. The model is based on a recently developed extended Navier-Stokes constitution that can be effectively used to describe the flows within KL [27], and the most appealing feature of the extended constitution is that it is derived rigorously and contains no empirical parameters. The rest of the paper is organized as follows. In Sec. II, we will give a brief description of the extended Navier-Stokes formulation. The LBE model with multiple effective relaxation times is present in Sec. III, and a kinetic boundary condition for the LBE is constructed and analyzed in Sec. IV. Some numerical tests are performed in Sec. V, and finally a summary is given in Sec. VI.

II. EXTENDED NAVIER-STOKES MODEL WITH KNUDSEN LAYER EFFECT

A. Generalized Navier-Stokes constitution

The Knudsen layer is the kinetic boundary layer formed when a gas flows over a solid surface (Fig. 1). The gas motion within the KL cannot be properly described by the Navier-Stokes equations because of the insufficient collisions in this region. In order to capture the KL while keeping the simple form of the Navier-Stokes model, Guo *et al.* proposed an extended Navier-Stokes formulation [27],

$$\boldsymbol{\tau}(\mathbf{r}) = -\mu_e(\mathbf{r})\dot{\boldsymbol{\gamma}}(\mathbf{r}), \tag{1}$$

where $\boldsymbol{\tau}(\mathbf{r})$, $\mu_e(\mathbf{r})$, and $\dot{\boldsymbol{\gamma}}(\mathbf{r})$ are the local shear stress, effective dynamic viscosity, and strain rate at position $\mathbf{r}$, respectively. The key point of this model lies in the definition of the effective viscosity μ_e. In Ref. [27] this was achieved by extending the relationship between the viscosity and the mean free path in the gas kinetic theory [4]

$$\lambda_e = \frac{\mu_e}{p}\sqrt{\frac{\pi RT}{2}}, \tag{2}$$

where $p=\rho RT$ is the pressure, with ρ the density, R the gas constant, and T the gas temperature. Therefore, once the effective mean-free-path λ_e is determined, the new Navier-Stokes model will be closed.

The effective mean free path λ_e in a gas system bounded by a solid wall is always smaller than that in an unbounded system, because the free paths of some molecules will be cut off by the wall. The effect of wall confinement on the mean free path can be expressed through a function Ψ,

$$\lambda_e = \lambda\Psi(\mathbf{r},\mathrm{Kn}). \tag{3}$$

The exact expression of Ψ can be derived rigorously through the probability distribution function of the free path of a gas molecule [27,28], and is usually dependent on the flow geometry. For instance, for a gas bounded between two parallel plates located at $y=0$ and $y=H$, respectively, the mean free path of the molecules in the plane located at $0 \leqslant y \leqslant H$ is [27]

$$\Psi(y) = \frac{1}{2}\left[\psi\left(\frac{y}{\lambda}\right) + \psi\left(\frac{H-y}{\lambda}\right)\right],$$

where λ is the mean free path for an unbounded system, and the function ψ is defined as

$$\psi(\alpha) = 1 + (\alpha - 1)e^{-\alpha} - \alpha^2 E_i(\alpha), \tag{4}$$

where $E_i(x)$ is the exponential integral function defined by

$$E_i(x) = \int_1^\infty t^{-1}e^{-xt}dt.$$

From Eqs. (2) and (3) we can obtain the effective geometry-dependent viscosity as

$$\mu_e(y) = \mu\Psi(y), \tag{5}$$

where μ is the viscosity for an unbounded gas or that far away from the wall.

It is noted that $\psi(x)$ is a monotonically increasing function satisfying $\psi(0)=0$ and $\psi(\infty)=1.0$. Therefore, if the top plate is removed, i.e., $H\to\infty$, the effective viscosity becomes

$$\mu_e(y) = \frac{\mu}{2}\left[\psi\left(\frac{y}{\lambda}\right) + 1\right].$$

This suggests that the effective viscosity will approach the bulk one far away from the wall, but is exactly one half of the bulk one at the wall. The fact that $\mu_e(0)=\mu/2$ is consistent with some previous independent studies [29,30].

For a more complicated geometry, the exact formulation of the geometric function $\Psi(\mathbf{r},\mathrm{Kn})$ may be quite complicated. However, if the local curvature of the wall is not large, a more effective way may be to use the present formulation as a "wall function," just the same as that proposed in Ref. [30]. It has been shown that this approach can indeed improve predictions within the KL [27]. Hereafter, we will call the model using the effective viscosity "generalized Navier-Stokes equations."

B. A generalized second-order slip boundary condition

In practical applications the generalized Navier-Stokes equations with the extended constitution must be supplemented by some suitable boundary conditions. As illustrated in Fig. 1, the true or microscopic velocity at the wall, u_s, is usually different from the virtual or macroscopic slip velocity u_s^{ns} extrapolated from the Navier-Stokes velocity in the bulk region. For instance, for the Kramer's problem these two slip velocities are given approximately by [40]

$$u_s = \frac{2-\sigma}{\sigma}(1-0.1817\sigma)\lambda[\partial_{\mathbf{n}}u]_{\mathrm{KL}}, \tag{6a}$$

$$u_s^{ns} = \frac{2-\sigma}{\sigma}(1+0.1621\sigma)\lambda[\partial_{\mathbf{n}}u]_{\mathrm{KL}}, \tag{6b}$$

where σ is the accommodation coefficient, $\mathbf{n}$ is the unit vector normal to the wall, and the subscript "KL" means evaluating the derivatives at the KL boundary. As $\sigma=1$, i.e., the wall is fully diffusive, both u_s and u_s^{ns} are in good agreement with the exact solutions of the linearized Boltzmann (BGK) equation [4]. The velocity outside the KL is linear for the Karmer's problem. Cercignani also proposed a second-order slip boundary condition for u_s^{ns} based on the solution of Boltzmann equation for the Poiseuille flow where the velocity outside the KL is nonlinear,

$$u_s^{ns} = \zeta\lambda'[\partial_{\mathbf{n}}u]_{\mathrm{wall}} - \frac{1}{2}\left(\frac{1}{2}+\zeta^2\right)\lambda'^2[\partial_{\mathbf{n}}^2 u]_{\mathrm{wall}}, \tag{7}$$

where $\zeta=1.016$ and $\lambda'=(2/\sqrt{\pi})\lambda$.

Motivated by Eqs. (6) and (7), in this work we propose a heuristic second-order slip boundary condition for the microscopic slip velocity u_s,

$$u_s := u(0) - u_w = A_1[\lambda_e\partial_{\mathbf{n}}u]_{\mathrm{wall}} - A_2[\lambda_e\partial_{\mathbf{n}}(\lambda_e\partial_{\mathbf{n}}u)]_{\mathrm{wall}}, \tag{8}$$

where $u(0)$ is the gas velocity at the wall, u_w is the wall velocity, and the two slip coefficients are given by

$$A_1 = \frac{2-\sigma}{\sigma}(1-0.1817\sigma), \quad A_2 = \frac{1}{\pi}+\frac{1}{2}A_1^2. \tag{9}$$

This is a generalization of the boundary condition proposed in Ref. [27] where the two parameters A_1 and A_2 were set to be 1.0 and 0.5, respectively. It should be emphasized that the mean free path appearing in the above boundary condition is a locally position-dependent variable. If we replace λ_e with the constant bulk mean free path λ, Eq. (8) is very similar to the second-order slip boundary condition that is widely used for the classical Navier-Stokes equations [3]. It is also noted that owing to the use of the local effective mean free path, the slip velocity given by Eq. (8) is smaller than that of the classical one given by Eq. (7) as $\sigma=1$. This is reasonable since the microslip velocity u_s is usually smaller than the extrapolated Navier-Stokes slip velocity u_s^{ns}. In Ref. [27] it has been shown that the generalized Navier-Stokes model together with the heuristic boundary condition can give good predictions for flows with a large Kn.

III. GENERALIZED LBE WITH MULTIPLE EFFECTIVE RELAXATION TIMES

The LBE tracks the evolution of the discrete distribution functions for the gas molecules,

$$f_i(\mathbf{x}+\mathbf{c}_i\delta_t, t+\delta_t) - f_i(\mathbf{x},t) = \Omega_i(f) + \delta_t\mathbf{F}_i, \quad i=0,1,\ldots,b-1, \tag{10}$$

where $f_i(\mathbf{x},t)$ is the distribution function associated with the gas molecules moving with the discrete velocity $\mathbf{c}_i$ at position $\mathbf{x}\in\mathcal{L}$ and time t ($\mathcal{L}$ is a regular lattice with a spacing δ_x); $\mathbf{F}_i$ is a forcing term accounting for the body force experienced by the molecules, and $\Omega_i(f)$ is the discrete collision operator. The most widely used collision operator in LBE is the single relaxation time or BGK model [31],

$$\Omega_i = -\frac{1}{\tau}[f_i - f_i^{(eq)}], \tag{11}$$

where $f_i^{(eq)}$ is the discrete equilibrium distribution function. Models with multiple relaxation times (MRT) were also proposed [32,33], where the collision operator is given by

$$\Omega_i = -\sum_j (\mathsf{M}^{-1}\mathsf{S}\mathsf{M})_{ij}[f_j - f_j^{(eq)}], \tag{12}$$

where M is a $b\times b$ transform matrix projecting the discrete distribution functions f_i onto the moment space $\mathsf{m}=\mathsf{M}\mathsf{f}$ where $\mathsf{f}=(f_0,f_1,\cdots,f_{b-1})^{\mathsf{T}}$, and $\mathsf{S}=\mathrm{diag}(\tau_0,\tau_1,\cdots,\tau_{b-1})^{-1}$ is a non-negative diagonal matrix with τ_i being the relaxation time for the ith moment. As $\tau_i=\tau$, the MRT model reduces to the BGK model. The equilibrium distribution function in either the BGK or the MRT model depends on the gas density, velocity, and temperature. For an isothermal system, the temperature appears only as a free parameter, and the density ρ and momentum $\rho\mathbf{u}$ in $f_i^{(eq)}$ are defined as

$$\rho = \sum_i f_i, \quad \rho\mathbf{u} = \sum_i \mathbf{c}_i f_i + \frac{\delta_t}{2}\mathbf{F}. \tag{13}$$

In both the BGK and MRT models, the discrete velocity set with sufficient symmetry and the relevant equilibrium distribution functions must be chosen appropriately so that the LBE is accurate for the intended fluid dynamics. In most of the available LBE models, these components are mainly designed for continuum flows that can be described by the Navier-Stokes equations. Since the aim of our LBE model is to solve the generalized Navier-Stokes equations described in the preceding section, we will also use the velocity set and equilibrium distribution functions employed in the standard LBE. For simplicity and without loss of generality, we shall consider the two-dimensional nine-velocity (D2Q9) MRT model in this work, where the velocity set is given by

$$\mathbf{c}_i = \begin{cases} (0,0)c, & i=0, \\ (\pm 1,0)c,\ (0\pm 1)c, & i=1-4, \\ (\pm 1,\pm 1)c, & i=5-8, \end{cases} \tag{14}$$

where $c=\delta x/\delta t$, which is taken to be the velocity unit (i.e., $c=1$) in this work.

Based on the discrete velocity vectors given by Eq. (14), we can define nine discrete velocity moments of the distribution function,

$$\mathsf{m} := \mathsf{M}\mathsf{f} = (\rho, e, \varepsilon, j_x, q_x, j_y, q_y, p_{xx}, p_{xy})^{\mathsf{T}}, \tag{15}$$

where $\mathsf{f}=(f_0,f_1,\cdots,f_8)^{\mathsf{T}}$. These moments have clear physical significances: $m_0=\rho$ is the density, $m_1=e$ are related to the total energy, $m_2=\varepsilon$ is related to energy square, $(m_3,m_5):=(j_x,j_y)$ are the momentum components, $(m_4,m_6):=(q_x,q_y)$ is related to the heat flux, and $m_7=p_{xx}$ and $m_8=p_{xy}$ are related to the diagonal and off-diagonal components

of the stress tensor, respectively. With the ordering of moments specified by Eq. (15), the relaxation times in the diagonal matrix S are given by

$$\mathsf{S} = \mathrm{diag}(\tau_\rho, \tau_e, \tau_\varepsilon, \tau_j, \tau_q, \tau_j, \tau_q, \tau_s, \tau_s)^{-1}, \tag{16}$$

and the corresponding transform matrix M for the D2Q9 model is given by

$$\mathsf{M} = \begin{pmatrix} 1 & 1 & 1 & 1 & 1 & 1 & 1 & 1 & 1 \\ -4 & -1 & -1 & -1 & -1 & 2 & 2 & 2 & 2 \\ 4 & -2 & -2 & -2 & -2 & 1 & 1 & 1 & 1 \\ 0 & 1 & 0 & -1 & 0 & 1 & -1 & -1 & 1 \\ 0 & -2 & 0 & 2 & 0 & 1 & -1 & -1 & 1 \\ 0 & 0 & 1 & 0 & -1 & 1 & 1 & -1 & -1 \\ 0 & 0 & -2 & 0 & 2 & 1 & 1 & -1 & -1 \\ 0 & 1 & -1 & 1 & -1 & 0 & 0 & 0 & 0 \\ 0 & 0 & 0 & 0 & 0 & 1 & -1 & 1 & -1 \end{pmatrix}. \tag{17}$$

The equilibrium distribution function in Eqs. (11) and (12) can be expressed as

$$f_i^{(eq)} = w_i \rho \left[1 + \frac{\mathbf{c}_i \cdot \mathbf{u}}{c_s^2} + \frac{(\mathbf{c}_i \cdot \mathbf{u})^2}{2c_s^4} + \frac{\mathbf{u} \cdot \mathbf{u}}{2c_s^2} \right], \tag{18}$$

where $w_0 = 4/9$, $w_{1\sim4} = 1/9$, and $w_{5\sim8} = 1/36$, and $c_s = c/\sqrt{3}$ is the sound speed. For consistency, the forcing terms F_i's should be given by

$$\mathsf{F} = \mathsf{M}^{-1}\left(\mathsf{I} - \frac{1}{2}\mathsf{S}\right)\mathsf{M}\bar{\mathsf{F}}, \tag{19}$$

where I is the unity matrix, $\mathsf{F} = (F_0, F_1, \cdots, F_8)^{\mathsf{T}}$, and $\bar{\mathsf{F}} = (\bar{F}_0, \bar{F}_1, \cdots, \bar{F}_8)^{\mathsf{T}}$ with

$$\bar{F}_i = w_i \left[\frac{\mathbf{c}_i \cdot \mathbf{F}}{c_s^2} + \frac{\mathbf{uF}:(\mathbf{c}_i\mathbf{c}_i - c_s^2\mathsf{I})}{c_s^4} \right]. \tag{20}$$

The forcing term given by Eq. (19) is a generalization of that for the BGK model as proposed in Ref. [34].

With the equilibria given by Eqs. (18) and the forcing term given by Eq. (19), the Navier-Stokes equations can be derived from the MRT-LBE,

$$\partial_t \rho + \nabla \cdot (\rho \mathbf{u}) = 0, \tag{21a}$$

$$\partial_t(\rho \mathbf{u}) + \nabla \cdot (\rho \mathbf{u}\mathbf{u}) = -\nabla p + \nabla \cdot [2\rho\nu\mathbf{S} + \rho\zeta(\nabla \cdot \mathbf{u})\mathsf{I}] + \mathbf{F}, \tag{21b}$$

where $p = c_s^2\rho = \rho RT$ is the pressure with T being the system temperature and R the gas constant, $S_{ij} = (\partial_i u_j + \partial_j u_i)/2$ is the strain rate, ν and ζ are the kinematic shear and bulk viscosities given by [33]

$$\nu = c_s^2\left(\tau_s - \frac{1}{2}\right)\delta_t, \quad \zeta = \frac{c_s^2}{2}\left(\tau_e - \frac{1}{2}\right)\delta_t. \tag{22}$$

Therefore, in order to solve the extended Navier-Stokes model with the LBE (10), the relaxation time τ_s should be chosen as

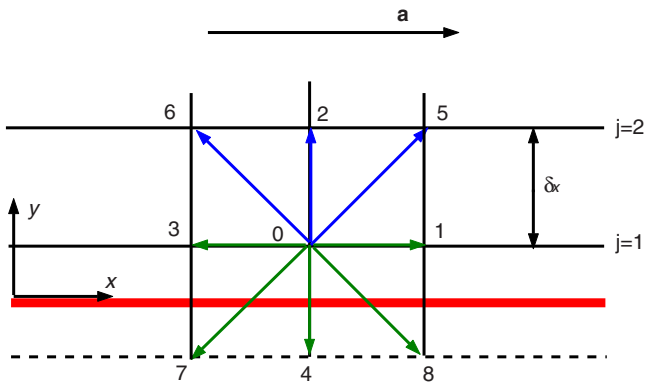

FIG. 2. (Color online) Schematic of the flow geometry and lattice arrangement.

$$\tau_s = \frac{1}{2} + \frac{\mu_e}{p\delta_t}, \tag{23}$$

which can also be rewritten in terms of the Knudsen number based on Eqs. (2) and (3) as

$$\tau_s = \frac{1}{2} + \sqrt{\frac{6}{\pi}} N\,\mathrm{Kn}\Psi(\mathbf{r}, \mathrm{Kn}), \tag{24}$$

where $N = h/\delta_x$ is the grid number in the direction of the characteristic length, and we have made use of the fact that $c = \sqrt{3RT} = 1$ for the LBE model in the deduction. The other relaxation times can be chosen with some freedom due to the decoupling between the relaxation processes of different moments [33].

IV. KINETIC BOUNDARY CONDITION FOR THE GENERALIZED LBE

A. The combined bounce-back and/or specular-reflection boundary condition

In practical applications, suitable boundary conditions must be supplied for the LBE. Some schemes have been proposed for the BGK-LBE in the literature, such as the discrete Maxwell's diffuse-reflection schemes [10,35] and the combined bounce-back and specular-reflection (CBBSR) schemes [17,36]. Recently, the two schemes were analyzed for both the BGK- and MRT-LBE with (a) constant relaxation time(s) [37,38], and it was found that they are identical in a parametric range and both contain some discrete effects.

In this work, we shall propose a generalized CBBSR model for the proposed MRT-LBE. For simplicity and without loss of generality, we consider a flat surface as sketched in Fig. 2. It is noted that the lattice is arranged so that the solid wall locates at $j = 1/2$, where j is the index of the grid line at $y_j = (j - 0.5)\delta_x$. After the collision substep at time t at every node, i.e.,

$$\tilde{f}_i(\mathbf{x}, t) = f_i(\mathbf{x}, t) + \Omega_i(\mathbf{x}, t) + \delta_t F_i,$$

the streaming substep,

$$f_i(\mathbf{x}+\mathbf{c}_i\delta_t,t+\delta_t)=\tilde{f}_i(\mathbf{x},t),$$

can be performed for all nodes at $j>1$. But for the nodes at $j=1$, only the distribution functions f_0^1, f_1^1, f_3^1, f_7^1, and f_8^1 can be determined after the streaming, the remaining distribution functions, f_2^1, f_5^1, and f_6^1, cannot be provided by the streaming step and must be specified according to the kinetic boundary condition at the wall. For the CBBSR boundary condition, they are given by

$$f_2^1=\tilde{f}_4^1+2r\rho\mathbf{c}_2\cdot\mathbf{u}_w/c_s^2,$$

$$f_5^1=r\tilde{f}_7^1+(1-r)\tilde{f}_8^1+2r\rho\mathbf{c}_5\cdot\mathbf{u}_w/c_s^2,$$

$$f_6^1=r\tilde{f}_8^1+(1-r)\tilde{f}_7^1+2r\rho\mathbf{c}_6\cdot\mathbf{u}_w/c_s^2 \tag{25}$$

where $0\leqslant r\leqslant 1$ is the portion of the bounce-back part in the combination. In the CBBSR scheme, the parameter r plays an important role in simulations. In most previous applications, r was chosen quite arbitrarily. But recently it was shown that even for the LBE with (a) constant relaxation time(s), r depends on a number of factors, including the Knudsen number, the lattice size, and the relaxation time(s), and it must be carefully chosen in order to obtain a reasonable solution [37,38]. It can be expected that for the present LBE with the locally changing relaxation time τ_s, the influences on r would be more complicated. In the subsequent subsection we will present an analysis of the CBBSR scheme to investigate this problem.

B. Analysis of the CBBSR scheme

To simplify the analysis, we consider the steady incompressible Poiseuille flow driven by a constant force $\mathbf{F}=(F_x,F_y)=\rho(a,0)$, where we assume that

$$\frac{\partial\phi}{\partial t}=0,\quad \rho=\text{const},\quad v=u_y=0,\quad \frac{\partial\phi}{\partial x}=0, \tag{26}$$

where ϕ is an arbitrary flow variable. Under such conditions, by expanding the left-hand side of the LBE (10) into a Taylor series in δ_t up to second order, we can obtain that

$$c_{iy}\partial_y f_i+\frac{\delta_t}{2}c_{iy}^2\partial_y^2 f_i=\Omega_i'(f)+F_i, \tag{27}$$

where $\Omega'=\mathsf{M}^{-1}\mathsf{S}'\mathsf{M}[\mathsf{f}-\mathsf{f}^{(\mathrm{eq})}]$ with $\mathsf{S}'=\mathsf{S}/\delta_t$. Multiplying both-hand sides of Eq. (27) by the matrix M, we can obtain the following equations for the moments:

$$\frac{\delta_t}{2}\partial_y^2\left[\frac{2\rho}{3}+\frac{e}{6}-\frac{p_{xx}}{2}\right]=0, \tag{28a}$$

$$\partial_y q_y+\frac{\delta_t}{2}\partial_y^2\left[\frac{2\rho}{3}+\frac{e}{2}+\frac{\varepsilon}{3}-\frac{p_{xx}}{2}\right]=-\frac{e+2\rho-3\rho\mathbf{u}^2}{\tau_e\delta_t}+\frac{6(\tau_e-0.5)\rho au}{\tau_e}, \tag{28b}$$

$$\partial_y q_y+\frac{\delta_t}{2}\partial_y^2\left[\frac{e}{3}+\frac{\varepsilon}{3}+p_{xx}\right]=-\frac{\varepsilon-\rho+3\rho u^2}{\tau_\varepsilon\delta_t}-\frac{6(\tau_\varepsilon-0.5)\rho au}{\tau_\varepsilon}, \tag{28c}$$

$$\partial_y p_{xy}+\frac{\delta_t}{2}\partial_y^2\left[\frac{2\rho u}{3}+\frac{q_x}{3}\right]=\rho a, \tag{28d}$$

$$\partial_y p_{xy}+\frac{\delta_t}{2}\partial_y^2\left[\frac{2\rho u}{3}+\frac{q_x}{3}\right]=-\frac{q_x+\rho u}{\tau_q\delta_t}-\frac{(\tau_q-0.5)\rho a}{\tau_q}, \tag{28e}$$

$$\partial_y\left[\frac{2\rho}{3}+\frac{e}{6}-\frac{p_{xx}}{2}\right]=0, \tag{28f}$$

$$\partial_y\left[\frac{e}{3}+\frac{\varepsilon}{3}+p_{xx}\right]+\frac{\delta_t}{2}\partial_y^2 q_y=-\frac{q_y}{\tau_q\delta_t}, \tag{28g}$$

$$\frac{1}{3}\partial_y q_y+\frac{\delta_t}{2}\partial_y^2\left[-\frac{2\rho}{9}+\frac{2}{18}+\frac{\varepsilon}{9}+\frac{p_{xx}}{2}\right]=-\frac{p_{xx}-\rho u^2}{\tau_s\delta_t}+\frac{(2\tau_s-1)\rho au}{\tau_s}, \tag{28h}$$

$$\partial_y\left[\frac{2\rho u}{3}+\frac{q_x}{3}\right]+\frac{\delta_t}{2}\partial_y^2 p_{xy}=-\frac{p_{xy}}{\tau_s\delta_t}. \tag{28i}$$

Equations (28d) and (28e) allow one to identify that

$$q_x=-\rho u-\left(2\tau_q-\frac{1}{2}\right)\rho a\delta_t, \tag{29}$$

while from Eqs. (28d) and (28i) we can obtain that

$$\partial_y\left[\frac{\tau_s-0.5}{\tau_s}p_{xy}\right]=\rho a+O(\delta_t^2), \tag{30a}$$

$$\partial_y\left[\frac{2\rho u}{3}+\frac{q_x}{3}+\frac{\delta_t\rho a}{2}\right]=-\frac{p_{xy}}{\tau_s\delta_t}+O(\delta_t^2). \tag{30b}$$

Equations (29) and (30) indicate that the LBE (10) is actually a second-order numerical scheme for the following equation:

$$\partial_y(\nu_e\partial_y u)-2\delta_t\partial_y(\nu_e a\partial_y\tau_q)=-a, \tag{31}$$

where $\nu_e=\frac{1}{3}(\tau_s-0.5)\delta_t$. It is noted that Eq. (31) is not the exact Navier-Stokes equation for the Poiseuille flow due to the second term on the left-hand side, which is nonzero in general. However, this term can be canceled in the proposed MRT-LBE by setting τ_q to be a constant, since the relaxation times can be chosen independently. Obviously, this is unreachable for the BGK-LBE model which uses a unique relaxation time.

The constant value of τ_q in the MRT-LBE can be determined from the boundary condition. Actually, some previous studies for the LBE with constant relaxation times [38,39] has shown that the choice of τ_q has a significant influence on the accuracy of a specific kinetic boundary condition. To see this point more clearly, now we make a detailed analysis for

the proposed CBBSR scheme. First, based on the relationship between the distribution functions f and the moments m, we have

$$f_1 - f_3 = \frac{1}{3}j_x - \frac{1}{3}q_x, \tag{32a}$$

$$f_5 - f_6 = \frac{1}{3}j_x + \frac{1}{6}q_x + \frac{1}{2}p_{xy}, \tag{32b}$$

$$f_8 - f_7 = \frac{1}{3}j_x + \frac{1}{6}q_x - \frac{1}{2}p_{xy}, \tag{32c}$$

from which we can obtain that

$$j_x = \rho u - \frac{\delta_t}{2}\rho a. \tag{33}$$

Similarly, we can also express the postcollision distribution functions as

$$\tilde{f}_1 - \tilde{f}_3 = \frac{1}{3}\tilde{j}_x - \frac{1}{3}\tilde{q}_x, \tag{34a}$$

$$\tilde{f}_5 - \tilde{f}_6 = \frac{1}{3}\tilde{j}_x + \frac{1}{6}\tilde{q}_x + \frac{1}{2}\tilde{p}_{xy}, \tag{34b}$$

$$\tilde{f}_8 - \tilde{f}_7 = \frac{1}{3}\tilde{j}_x + \frac{1}{6}\tilde{q}_x - \frac{1}{2}\tilde{p}_{xy}, \tag{34c}$$

where the postcollision moments are given by

$$\tilde{m}_k = m_k - \frac{1}{\tau_k}[m_k - m_k^{(eq)}] + \hat{F}_k\delta_t, \tag{35}$$

for $k=0,1,\ldots,8$, where the equilibrium moments and the corresponding forcing term in the moment space are given by $\mathsf{m}^{(eq)}=\mathsf{M}\mathsf{f}^{(eq)}$ and $\hat{\mathsf{F}}=\mathsf{M}\mathsf{F}=(\mathsf{I}-\mathsf{S}/2)\hat{\bar{F}}$, respectively. Under the conditions given by Eq. (26), we have

$$j_x^{(eq)} = \rho u, \quad q_x^{(eq)} = -\rho u, \quad p_{xy}^{(eq)} = 0, \tag{36}$$

and

$$\hat{\bar{F}}_{j_x} = \rho a, \quad \hat{\bar{F}}_{q_x} = -\rho a, \quad \hat{\bar{F}}_{p_{xy}} = 0. \tag{37}$$

With these results, we can obtain from Eq. (35) that

$$\tilde{j}_x = \left(1 - \frac{1}{\tau_j}\right)j_x + \frac{\rho u}{\tau_j} + \left(1 - \frac{1}{2\tau_j}\right)\rho a\delta_t, \tag{38a}$$

$$\tilde{q}_x = \left(1 - \frac{1}{\tau_q}\right)q_x - \frac{\rho u}{\tau_q} - \left(1 - \frac{1}{2\tau_q}\right)\rho a\delta_t, \tag{38b}$$

$$\tilde{p}_{xy} = \left(1 - \frac{1}{\tau_s}\right)p_{xy}. \tag{38c}$$

Furthermore, the unidirectional property of the flow suggests that

$$f_1 - f_3 = \tilde{f}_1 - \tilde{f}_3. \tag{39}$$

Then, from Eqs. (32a), (33), (34a), (38), and (39) we can obtain that

$$q_x = -\rho u - \left(2\tau_q - \frac{1}{2}\right)\rho a\delta_t, \tag{40a}$$

$$\tilde{j}_x = \rho u + \frac{\rho a\delta_t}{2}, \tag{40b}$$

$$\tilde{q}_x = -\rho u - \left(2\tau_q - \frac{3}{2}\right)\rho a\delta_t. \tag{40c}$$

With these results at hand, we can now investigate the slip velocity u_s at the wall corresponds to the CBBSR scheme. First, it is noted that the distribution functions at $j=1$ and 2 have the following relationship (see Fig. 2):

$$f_5^{(2)} - f_6^{(2)} = \tilde{f}_5^{(1)} - \tilde{f}_6^{(1)}, \quad f_8^{(1)} - f_7^{(1)} = \tilde{f}_8^{(2)} - \tilde{f}_7^{(2)}, \tag{41}$$

where $f_i^{(j)}=f_i(y_j)$, which gives that

$$p_{xy}^{(1)} = \frac{\tau_s^{(1)}[(2\tau_s^{(2)} - 1)(\rho u_1 - \rho u_2) - 3\rho a\delta_t]}{3[\tau_s^{(1)} + \tau_s^{(2)} - 1]}, \tag{42}$$

where $u_j=u(y_j)$, and we have made use of the assumption that τ_q is a constant. On the other hand, the CBBSR scheme (25) gives that

$$f_5^{(1)} - f_6^{(1)} = (1-2r)[\tilde{f}_8^{(1)} - \tilde{f}_7^{(1)}]. \tag{43}$$

With the aid of Eqs. (32b)–(42), we can obtain from the above equation that

$$u_2 = Au_1 + B\delta_t a, \tag{44}$$

where

$$A = \frac{2(r-1)\tilde{\tau}_s^{(1)}\tilde{\tau}_s^{(2)} - r(\tilde{\tau}_s^{(1)} + 2\tilde{\tau}_s^{(2)})}{\tilde{\tau}_s^{(2)}[2(r-1)\tilde{\tau}_s^{(1)} - r]}, \tag{45}$$

$$B = \frac{4r(\tilde{\tau}_s^{(1)} + \tilde{\tau}_s^{(2)})\tilde{\tau}_q + (9-11r)\tilde{\tau}_s^{(1)} + (3-5r)\tilde{\tau}_s^{(2)} + 3r}{2\tilde{\tau}_s^{(2)}[2(r-1)\tilde{\tau}_s^{(1)} - r]},$$

where $\tilde{\tau}_s^{(j)}=\tau_s(y_j)-0.5$ and $\tilde{\tau}_q=\tau_q-0.5$.

By expanding u_1 and u_2 around $y=0$ up to $O(\delta_x^2)$, respectively and making use of Eq. (31) with τ_q=const, we can obtain the slip velocity u_s from Eq. (44) as

$$u_s = u(0) = L_1\delta_x u'(0) - L_2\delta_x^2 u''(0), \tag{46}$$

where $u'=\partial_y u$ and $u''=\partial_y^2 u$, and

$$L_1 = \frac{3A - 9 - 2B\tilde{\tau}_s'(0)\delta_x}{6(1-A)}, \quad L_2 = \frac{27 - 3A + 8B\tilde{\tau}_s^{(0)}}{24(1-A)}, \tag{47}$$

where $\tilde{\tau}_s'=\partial_y\tilde{\tau}_s$. With this result, we can now realize the generalized second-order slip boundary condition (8) with the CBBSR scheme by properly choosing the parameter r and the relaxation time τ_q. To this end, we first rewrite the heuristic boundary condition (8) as

$$u_s = [A_1 - A_2\lambda_e'(0)]\lambda_e(0)u'(0) - A_2\lambda_e^2(0)u''(0). \quad (48)$$

Then, from the relation between the mean free path and the lattice spacing, $\lambda_e(0)=\chi\tilde{\tau}_s(0)\delta_x$ where $\chi=\sqrt{\pi/6}$, we reexpress Eq. (48) as

$$u_s = [A_1 - A_2\lambda_e'(0)]\chi\tilde{\tau}_s(0)\delta_x u'(0) - A_2\chi^2\tilde{\tau}_s^2(0)\delta_x^2 u''(0). \quad (49)$$

Comparing Eq. (49) with Eq. (46), we can see that in order to realize the boundary condition (8) with the CBBSR scheme, the parameter r and the relaxation time τ_q must satisfy the following two constraints:

$$L_1 = [A_1 - A_2\lambda_e'(0)]\chi\tilde{\tau}_s(0), \quad L_2 = A_2\chi^2\tilde{\tau}_s^2(0). \quad (50)$$

The solution of the above equation is very tedious due to the nonconstant relaxation time τ_s. To simplify the algebra, we expand $\tau_s^{(1)}$ and $\tau_s^{(2)}$ around $y=0$ up to $O(\delta_x)$, and neglect all terms of $O(\delta_x^2)$ in Eq. (50). With such approximations, we finally obtain that

$$r = \left[1 + \chi A_1 + \frac{\tau_s'(0)\delta_x}{8\tilde{\tau}_s^2(0)}\right]^{-1}, \quad (51a)$$

$$\tilde{\tau}_q = \frac{3 + 24\chi^2\tilde{\tau}_s^2(0)A_2}{16\tilde{\tau}_s(0)} + \frac{\tau_s'(0)\delta_x[12 + 30\tilde{\tau}_s(0)\chi A_1]}{16\tilde{\tau}_s^2(0)}. \quad (51b)$$

It can be seen that as the relaxation time τ_s is a constant, the second terms in Eqs. (51a) and (51b) vanish, and the results are in agreement with the previous results for the standard MRT-LBE [38]. But for the present model these terms should be included since τ_s changes locally.

V. NUMERICAL RESULTS

The MRT-LBE (10), where the relaxation times τ_s and τ_q are determined from Eqs. (24) and (51b), respectively, together with the CBBSR boundary condition (25) where r is determined from Eq. (51a), are tested in this section by applying it to several typical microscale gas flows. In all of the following simulations, we use $A_1=\frac{2-\sigma}{\sigma}(1-0.1817\sigma)$ and $A_2=\pi^{-1}+A_1^2/2$, where σ is the accommodation coefficient. The relaxation times are set as follows: τ_s is determined by the Knudsen number given by Eq. (24), τ_q is given by Eq. (51b), $\tau_\rho=\tau_j=1$ for the conserved variables, and the remains are given by $\tau_e=1.1$ and $\tau_\varepsilon=1.2$. Actually we found that the relaxations times except for τ_s and τ_q have negligible influences on the simulation results.

A. Test of accuracy

We first test the accuracy of the proposed MRT-LBE by simulating the force-driven Poiseuille flow between two parallel plates. The boundary condition (25) are applied to the two walls which are assumed to be fully diffusive ($\sigma=1.0$), and periodic boundary conditions are applied to the inlet and exit of the channel. In our simulations we use a lattice with size $N_y\times 4$, where N_y is doubled from 4 to 512 successively.

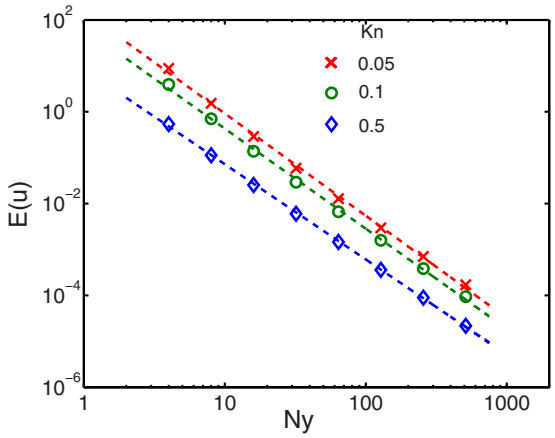

FIG. 3. (Color online) L_2 error $E(u)$ vs the grid number N_y in the y direction.

The driven force a is set to be 10^{-7} so that the Mach number is sufficiently small even for a finite Knudsen number.

In order to measure the relative error of the MRT-LBE, we first try to obtain a reference velocity by solving the Navier-Stokes equations with the effective viscosity given by Eq. (5). For the unidirectional Poiseuille flow, the Navier-Stokes equations reduce to

$$\frac{\partial}{\partial y}\left[\mu_e\frac{\partial u}{\partial y}\right] + \rho a = 0,$$

which can be integrated effectively using a standard numerical quadrature. Here we use the trapezoidal rule with 4096 points which gives the grid-independent reference result. After obtaining the reference velocity u_r, the relative L_2 error of the LBE result can be defined as

$$E(u) = \frac{\|u_{LBE} - u_r\|_2}{\|u_r\|_2}, \quad (52)$$

where u_{LBE} is the LBE result on a certain grid.

In Fig. 3 the L_2 errors of the LBE at several Kn. The slopes of the linear fittings for the cases of Kn=0.05, 0.1, and 0.5 are 2.227, 2.180, and 2.074, respectively. This fact indicates that the present MRT-LBE is a second-order scheme for the Navier-Stokes equations, which is consistent with our previous theoretical analysis.

B. Kramer problem

Now we apply the proposed MRT-LBE to the Kramer problem to demonstrate its capability for capturing the Knudsen layer. In this problem the gas fills the half space $y>0$ bounded by a wall in the plane $y=0$ and is sheared by a uniformly applied stress a at infinity [4]. For this problem, the second term on the right-hand side of the heuristic boundary condition (8) takes no effect since $\partial_y(\lambda_e\partial_y u)=0$ everywhere, and therefore equation (8) essentially gives a first-order slip boundary condition. In our simulations we did find that A_2 has no influence on the results.

In our simulations, the computational domain is $0\leqslant y \leqslant 20\lambda'$ where $\lambda'=(2/\sqrt{\pi})\lambda$, and a $N_y\times N_x=128\times 4$ lattice is

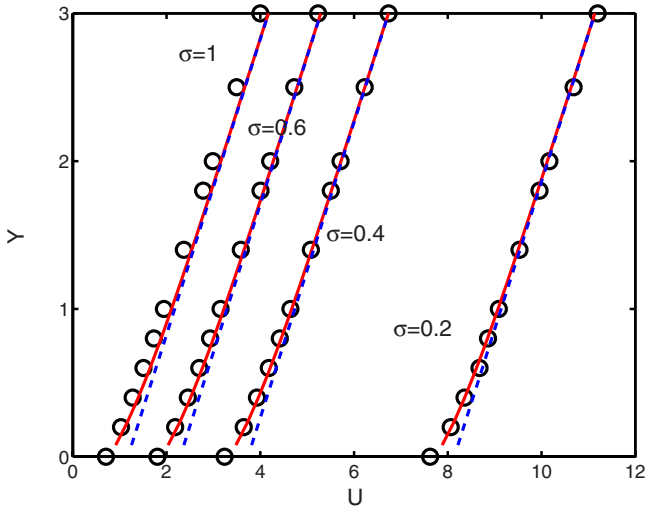

FIG. 4. (Color online) Velocity profiles of the Kramer problem. Solid line: MRT-LBE; dashed line: linear extrapolation; Symbol: linearized Boltzmann equation [40]. Here $Y=y/\lambda'$ with $\lambda'=(2/\sqrt{\pi})\lambda$, and $U=u/a\sqrt{2RT}$.

used so that the Knudsen layer can be well captured. Periodic boundary conditions are applied to the left and right boundaries, and the proposed CBBSR boundary condition is applied to the bottom wall, while the no-slip bounce-back scheme is applied to the upper infinite boundary moving with a velocity $u_\infty=u_{N_y-1}+a\delta_x/2$.

In Fig. 4, the velocity profiles predicted by the present MRT-LBE as σ changes from 0.2 to 1.0 are shown and compared with the results of the linearized Boltzmann equation [40]. For comparison, the linear extrapolations from the velocity profiles outside the KL are also shown. It is clearly seen that the LBE results are in good agreement with the solutions of the Boltzmann equation, and the nonlinearity of the velocity profile within the Knudsen layer is successfully captured. These observations demonstrate the potential capability of the present MRT-LBE model for capturing the flows within KL.

C. Couette flow

The present MRT-LBE is also applied to the Couette flow between two parallel plates with a distance H. The bottom plate located at $y=0$ is kept stationary, and the top one located at $y=H$ moves with a constant velocity u_w. In our simulations, the channel height is set to be $H=1.0$, and the mean free path is determined from the Knudsen number Kn, which ranges from 0.01 to 1.5. All simulations are performed on a $N_y\times N_x=128\times 4$ lattice, and periodic boundary conditions are again applied to the inlet and outlet of the channel, and the CBBSR scheme is applied to the both plates. It is again found that A_2 has no influence on the simulation for this problem.

In Fig. 5, the velocity profile at Kn=0.01 is shown and compared with the results of the direct simulation Monte Carlo (DSMC), the standard MRT-LBE, and the classical Navier-Stokes equations with a first-order slip boundary condition, $u_{\text{wall}}-u_w=\pm\lambda\partial_y u|_{\text{wall}}$, where the signs $\pm$ are for the

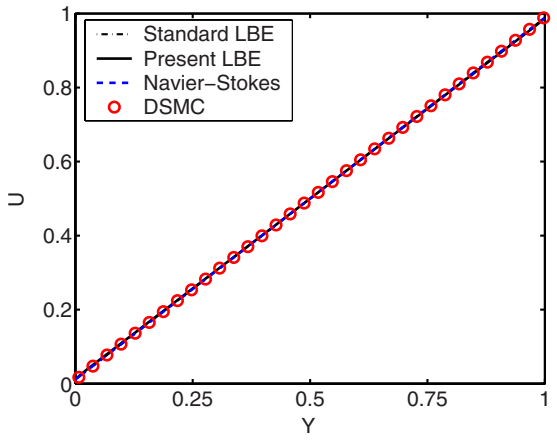

FIG. 5. (Color online) Velocity profile of the Couette flow at Kn=0.01. Here $Y=y/H$ and $U=u/u_w$.

bottom and top plates, respectively. Clearly, with this small Knudsen number the standard LBE, the present LBE, and the Navier-Stokes model all predict a linear velocity profile that agrees well with the DSMC data, and no obvious slip is observed. The indistinguishable velocity profiles indicate that the present LBE is equivalent to the standard LBE for the classical Navier-Stokes equations for small Knudsen number flows.

As shown in Fig. 6, apparent slip appears at both walls with the increasing Kn. It is first noted that the velocity profiles predicted by the standard LBE and the classical Navier-Stokes model are totally indistinguishable in all cases, and both are linear in the whole region. On the contrary, the present MRT-LBE and the DSMC both give nonlinear velocity profiles, although some discrepancies are observed for higher Kn. Specifically, at Kn=0.1, the predictions of the present LBE and the standard LBE (also the Navier-Stokes model) show some slight differences, but both are still in good agreement with the DSMC result. As Kn reaches to 0.25, the DSMC velocity profile becomes nonlinear near the two walls, and the present LBE gives better predictions than the standard LBE and Navier-Stokes within the two KLs. For further larger Kn ($0.25<\text{Kn}\leqslant 1.0$), it is clearly seen that the degree of slip increases with increasing Kn, and the standard LBE and/or Navier-Stokes solutions start to deviate from DSMC data more and more obviously, while those of the present LBE are much better. These observations further demonstrate the potential of the present LBE for capturing the KL and the capability for simulating moderate Kn flows. However, it is observed that at Kn=1.5, the present LBE underpredicts the slip velocity obviously. One possible reason for this deviation could be the heuristic slip boundary condition (8), which is motivated by the solution of the Kramer problem where only one KL is involved. For the Couette flow between two parallel plates, the two KL will overlap for larger Kn and thus the boundary condition will be inaccurate. More elegant boundary conditions that can treat overlapping KLs are still desirable.

D. Poiseuille flow

Both the Kramer and the Couette flows are driven by an applied shear stress, and the velocity profiles are linear out-

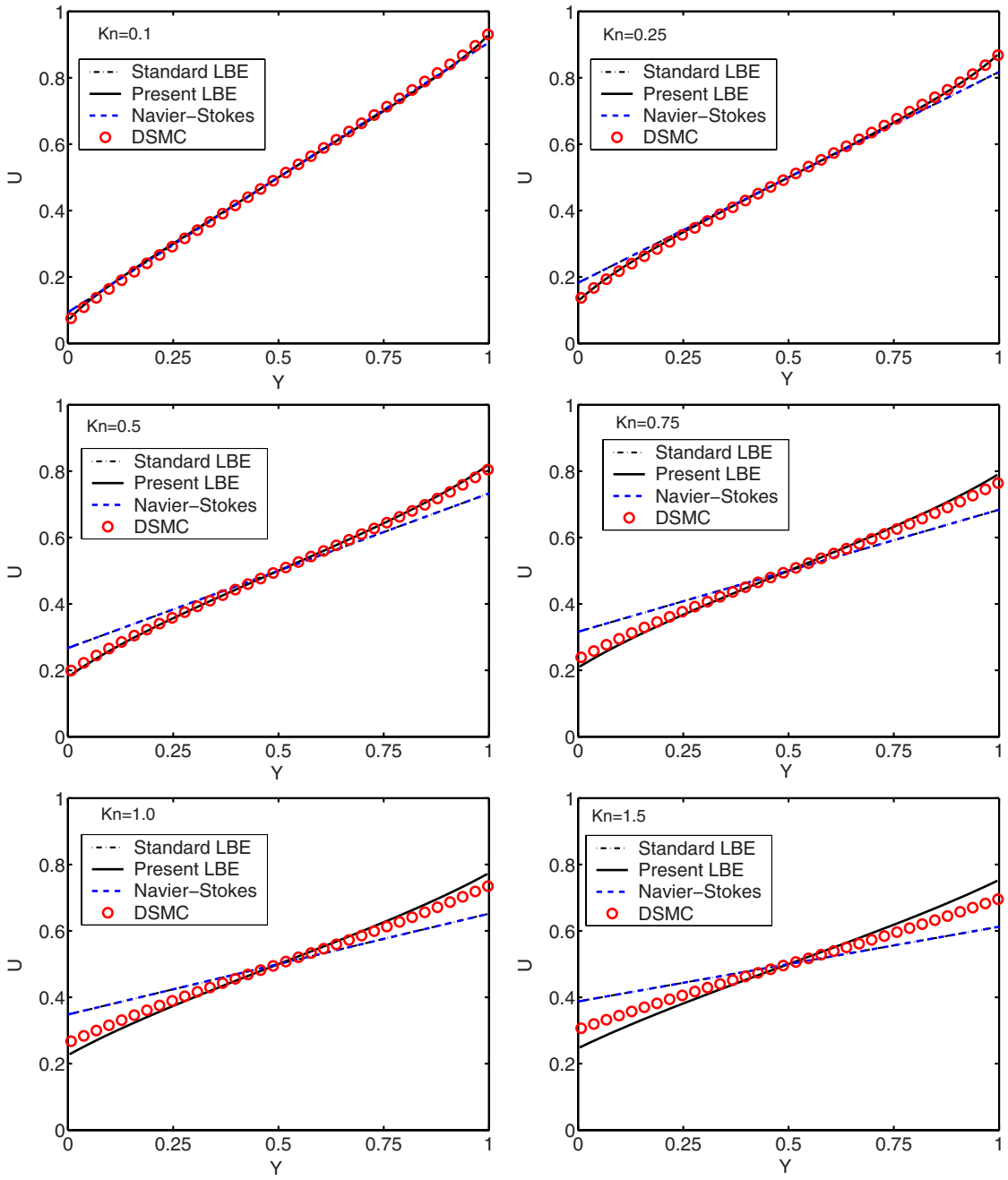

FIG. 6. (Color online) Velocity profile of the Couette flow at moderate Kn. Here $Y=y/H$ and $U=u/u_w$.

side the KLs. Now we consider the planar Poiseuille flow driven by a constant force a, which has a nonlinear velocity profile in the whole region. In all of the following simulations, we use the same parameters and boundary conditions as those used in the Couette flow. For comparison, the standard MRT-LBE using the second-order slip boundary condition but with different slip coefficients are also applied to the flow under the same condition. Here we use the term "LBE-1" to denote the standard LBE using $A_1=1.1466$ and $A_2=0.9795$ as proposed by Cercignani [4], and "LBE-2" to denote that using $A_1=1.11$ and $A_2=0.61$ as proposed by Hadjiconstantinou [42] which is an improved version of the Cercignani's.

In Fig. 7 the velocity profiles normalized by $u_r=aH(2/RT)^{1/2}$ at $\mathrm{Kn}=2k/\sqrt{\pi}$ with k ranging from 0.1 to 10 are compared with the solutions of the linearized Boltzmann equation [41]. It is seen that at $k=0.1$ (Kn=0.1128), the three LBE profiles are all in good agreement with the solution of the Boltzmann equation, although it can still be observed that the present LBE gives the best prediction. As k increases to 0.2, the LBE-1 gives an obvious overestimation in the whole region; The LBE-2, on the other hand, gives a good prediction in the central region, but the Knudsen layers near the two walls are not well captured; The present LBE, interestingly, provides a satisfied result in the whole region, especially within the two KLs.

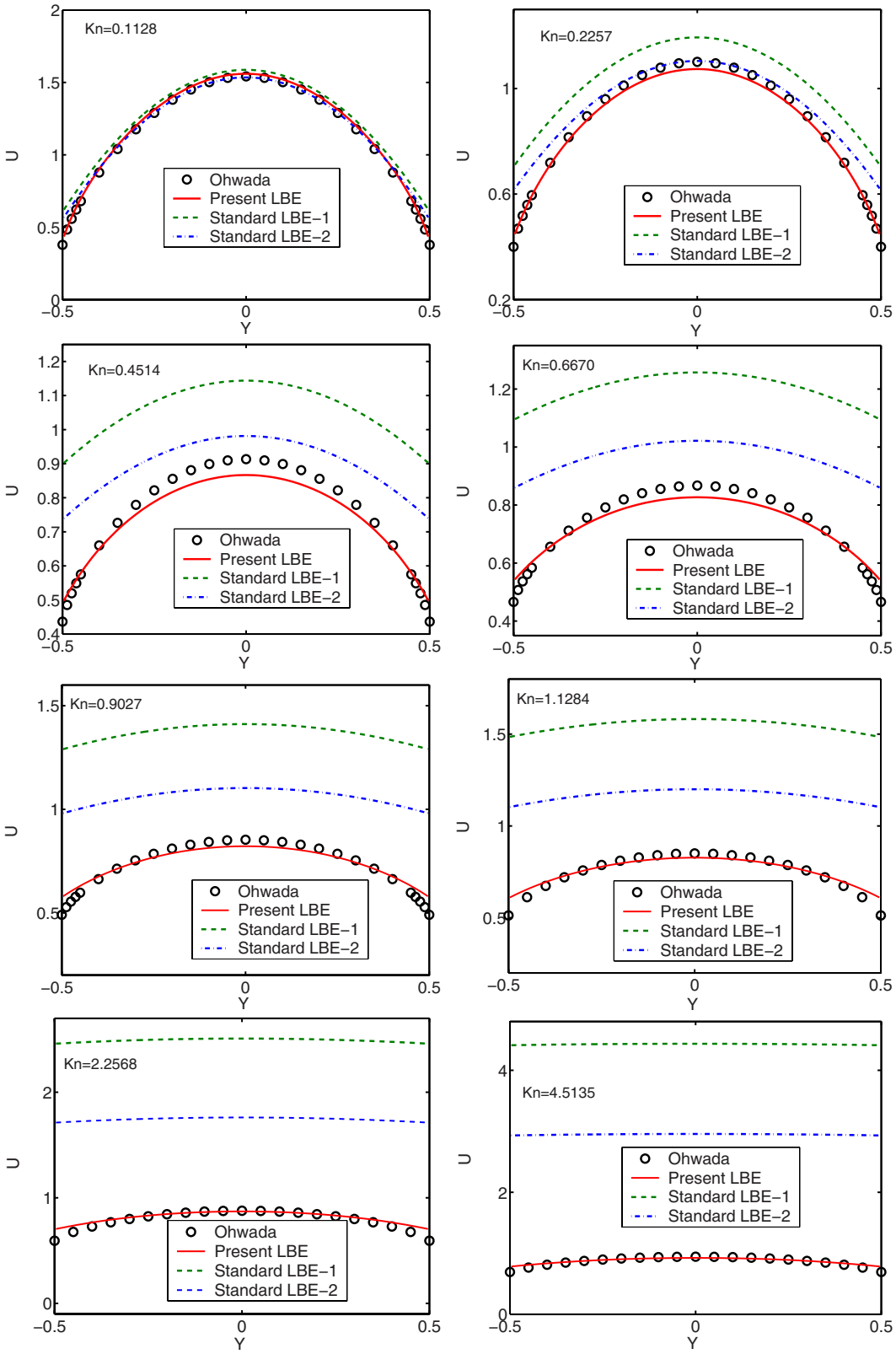

FIG. 7. (Color online) Velocity profile of the Poiseuille flow at moderate Kn. Here $Y=y/H$ and $U=u/u_r$.

For further larger Knudsen numbers, the results of LBE-1 depart from the solutions of the Boltzmann equation more and more, and becomes unuseful totally. For LBE-2, also over-predicts the velocity in the whole region and the deviation from the Boltzmann solution increases with increasing Kn. Encouragingly, the present LBE yields much better solutions than both the LBE-1 and LBE-2, and can still give a satisfactory prediction even as $k=4$.

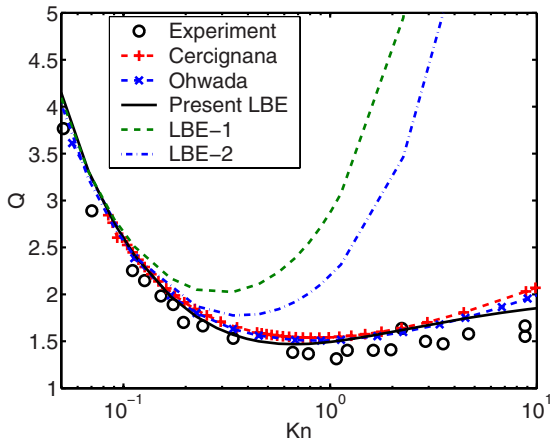

FIG. 8. (Color online) Mass flux of the Poiseuille flow against the Knudsen number.

To further demonstrate the advantage of the present LBE, in Fig. 8 we show the nondimensional mass fluxes Q of several methods normalized by $\rho a H^2/\sqrt{2RT}$. It is seen that all of the three LBEs give accurate mass fluxes as $\mathrm{Kn} \leqslant 0.1$ in comparison with the solutions of the Boltzmann equation obtained by different methods [4,41], and the experimental results for different gases [43]. Above this Kn, LBE-1, which uses the standard LBE that actually solves the Navier-Stokes equation together with the traditional second-order slip boundary condition suggested by Cercignani [4], fails to work any more. LBE-2, although gives improved result compared with LBE-1, also produces very unreasonable results as $\mathrm{Kn} > 0.3$. On the other hand, the present LBE predicts satisfied results in a rather larger region and is able to capture the Knudsen minimum successfully.

VI. SUMMARY

Based on a recently developed generalized Navier-Stokes model, we proposed a lattice Boltzmann equation with multiple effective relaxation times in which the wall-confinement effects are considered. A kinetic boundary condition (CBBSR) that combines the bounce-back and specular-reflection schemes was proposed for the LBE, and was analyzed based on a unidirectional flow. It was shown that in order to recover the generalized Navier-Stokes equations correctly, the relaxation time for the heat flux mode, τ_q, must be chosen to be a constant, which is determined from the boundary condition and the relaxation time τ_s for the shear mode. Furthermore, it is found that the bounce-back portion r in the CBBSR boundary condition depends on both the hydrodynamic boundary condition and τ_s.

One of the advantages of the present LBE is that it is still within the framework of the LBE for the Navier-Stokes equations, and thus shares the same advantages of the standard LBE. Another important feature of the present LBE is that it has the potential to capture the Knudsen layer by employing the geometry-dependent relaxation time τ_s. Some numerical simulations, although preliminary, demonstrate the potentials of the present LBE for microscale gas flows at moderate Knudsen numbers.

Finally, we would like to point out that the proposed CBBSR boundary condition is designed and analyzed for plane walls that are parallel to a particle velocity. For more general cases, however, it would be a nontrivial task to design a suitable boundary condition, and actually deserves another paper as done in Ref. [44]. We would like to extend the present method to cases involving curved boundaries in future work.

ACKNOWLEDGMENTS

Z.G. is grateful to Professor Kun Xu for many helpful discussions. He also thanks Dr. Hongwei Liu for providing the DSMC data of the Couette flow. This work is supported by the National Natural Science Foundation of China (Contract No. 50606012) and the National Basic Research Program of China (Contract No. 2006CB705804).

[1] C. M. Ho and Y. C. Tai, Annu. Rev. Fluid Mech. **30**, 579 (1998).
[2] D. J. Beebe, G. A. Mensing, and G. M. Walker, Annu. Rev. Biomed. Eng. **4**, 261 (2002).
[3] G. E. Karniadakis and A. Beskok, *Micro Flows, Fundamentals and Simulation* (Springer, New York, 2001).
[4] C. Cercignani, *Mathematical Methods in Kinetic Theory* (Plenum, New York, 1990).
[5] K. Xu, Phys. Fluids **14**, L17 (2002).
[6] K. Xu, Phys. Fluids **15**, 2077 (2003); K. Xu and Z. Li, J. Fluid Mech. **513**, 87 (2004); T. Ohwada and K. Xu, J. Comput. Phys. **201**, 315 (2004).
[7] X. Nie, G. D. Doolen, and S. Chen, J. Stat. Phys. **107**, 279 (2002).
[8] C. Y. Lim *et al.*, Phys. Fluids **14**, 2299 (2002).
[9] A. Agrawal, L. Djenidi, and R. A. Antonia, J. Fluid Mech. **530**, 135 (2005).
[10] G. Tang, W. Tao, and Y. He, Phys. Fluids **17**, 058101 (2005).
[11] V. Sofonea and R. F. Sekerka, J. Comput. Phys. **207**, 639 (2005).
[12] V. Sofonea and R. F. Sekerka, Phys. Rev. E **71**, 066709 (2005).
[13] T. Lee and C. L. Lin, Phys. Rev. E **71**, 046706 (2005).
[14] S. Ansumali, C. E. Frouzakis, I. V. Karlin, and I. G. Kevrekidis, e-print arXiv:cond-mat/0502018.
[15] X. Niu, C. Shu, and Y. T. Chew, Europhys. Lett. **67**, 600 (2004).
[16] F. Toschi and S. Succi, Europhys. Lett. **69**, 549 (2005).
[17] M. Sbragaglia and S. Succi, Phys. Fluids **17**, 093602 (2005).
[18] Y. Zhang, R. Qin, and D. R. Emerson, Phys. Rev. E **71**, 047702 (2005).
[19] S. S. Chikatamarla and I. V. Karlin, Phys. Rev. Lett. **97**, 190601 (2006).
[20] Y. H. Zhang, X. J. Gu, R. W. Barber, and D. R. Emerson, Phys.

Rev. E **74**, 046704 (2006); Europhys. Lett. **77**, 30003 (2007).
[21] Z. L. Guo, T. S. Zhao, and Y. Shi, J. Appl. Phys. **99**, 074903 (2006).
[22] X. Shan, X.-F. Yuan, and H. Chen, J. Fluid Mech. **550**, 413 (2006).
[23] X. He and L.-S. Luo, Phys. Rev. E **55**, R6333 (1997); **56**, 6811 (1997).
[24] X. Shan and X. He, Phys. Rev. Lett. **80**, 65 (1998).
[25] R. Zhang, X. Shan, and H. Chen, Phys. Rev. E **74**, 046703 (2006).
[26] X. Niu, S. A. Hyodo, T. Munekata, and K. Suga, Phys. Rev. E **76**, 036711 (2007).
[27] Z. L. Guo, B. C. Shi, and C. G. Zheng, Europhys. Lett. **80**, 24001 (2007).
[28] D. W. Stops, J. Phys. D **3**, 685 (1970).
[29] M. Fichman and G. Hetsroni, Phys. Fluids **17**, 123102 (2005).
[30] D. A. Lockerby, J. M. Reese, and M. A. Gallis, AIAA J. **43**, 1391 (2005).
[31] Y. Qian, D. d'Humières, and P. Lallemand, Europhys. Lett. **17**, 479 (1992).
[32] D. d'Humières, in *Rarefied Gas Dynamics: Theory and Simulations*, edited by B. D. Shizgal and D. P. Weaver, Progress in Astronautics and Aeronautics No. 159 (AIAA, Washington, DC, 1992), pp. 450–458.
[33] P. Lallemand and L.-S. Luo, Phys. Rev. E **61**, 6546 (2000).
[34] Z. L. Guo, C. G. Zheng, and B. C. Shi, Phys. Rev. E **65**, 046308 (2002).
[35] S. Ansumali and I. V. Karlin, Phys. Rev. E **66**, 026311 (2002).
[36] S. Succi, Phys. Rev. Lett. **89**, 064502 (2002).
[37] Z. L. Guo, B. C. Shi, T. S. Zhao, and C. G. Zheng (unpublished).
[38] Z. L. Guo and C. G. Zheng, in *Proceedings of the 4th International Conference on Mesoscopic Methods in Engineering and Science*, 2007 (unpublished).
[39] I. Ginzburg and D. d'Humières, Phys. Rev. E **68**, 066614 (2003).
[40] S. K. Loyalka, N. Petrellis, and T. S. Strovick, Phys. Fluids **18**, 1094 (1975).
[41] T. Ohwada, Y. Sone, and K. Aoki, Phys. Fluids A **1**, 2042 (1989).
[42] N. G. Hadjiconstantinou, Phys. Fluids **15**, 2352 (2003).
[43] W. Dong, University of California Report No. UCRL-3353, 1956 (unpublished).
[44] L. Szalmas, Int. J. Mod. Phys. C **18**, 15 (2007); Phys. Rev. E **73**, 066710 (2006).